Available online at www.sciencedirect.com
ScienceDirect
Journal of Marine Systems 66 (2007) 122–129
JOURNAL OF MARINE SYSTEMS
www.elsevier.com/locate/jmarsys

Effect of wave boundary layer on sea-to-air dimethylsulfide transfer velocity during typhoon passage

Peter C. Chu *, Kuo-Feng Cheng

Naval Ocean Analysis and Prediction Laboratory, Naval Postgraduate School, Monterey, California, USA

Received 22 October 2005; accepted 13 January 2006
Available online 7 September 2006

Abstract

A full-spectral third-generation ocean wind–wave model (Wavewatch-III) implemented in the South China Sea is used to investigate the effects of the wave boundary layer on the drag coefficient and the sea-to-air transfer velocity of dimethylsulfide (DMS) during passage of Typhoon Wukong (September 5–11, 2000) with a maximum sustained wind speed of 38 m s^{-1}. The model is driven by the reanalyzed surface winds (1° × 1°, four times daily) from the National Centers for Environmental Prediction. It is found that the wave boundary layer evidently enhances (16.5%) the drag coefficient (in turn increases the momentum flux across the air–sea interface), and reduces (13.1%) the sea-to-air DMS transfer velocity (in turn decreases the sea-to-air DMS flux). This indicates the possibility of important roles of wave boundary layer in atmospheric DMS contents and global climate system.

Keywords: Dimethylsulfide; Sea-to-air gas transfer velocity; Wave boundary layer; Tropical cyclone; Drag coefficient; Wavewatch-III; South China Sea

1. Introduction

The dominant natural source of sulfur to the atmosphere is the oceanic dimethylsulfide (DMS) (Bates et al., 1992; Gondwe et al., 2003). In the atmosphere, DMS is oxidized to sulfuric and methanesulfonic acids which condense to form new aerosol particles and/or to add mass to existing particles. These particles can affect the Earth's radiation budget by scattering solar radiation back to space and altering the properties and lifetimes of clouds. In estimation of the Earth's radiation budget, the sea-to-air DMS flux must be included in the chemical transport and climate models in order to accurately calculate aerosol radiative forcing. The sea-to-air DMS flux depends on airside and waterside transfer velocities.

A moving tropical cyclone is an intense source of surface wind stress that produces strong ocean waves which changes the surface momentum flux and sea-to-air DMS transfer velocity. Up until now, effect of wave boundary layer (WBL) on the surface momentum flux through drag coefficient C_D and roughness length z_0 has been investigated over small areas of the sea or in wave tanks (Hwang, 2005), but not over regional seas with high waves forced by strong winds such as by tropical cyclones. However, effect of WBL on the sea-to-air DMS transfer velocity has not yet been investigated. In this paper, we study the effects of WBL on (C_D, z_0) and sea-to-air DMS transfer velocity in the South China Sea (SCS) during the passage of Typhoon Wukong (September 4–10, 2000).

* Corresponding author. Tel.: +1 831 656 3688; fax: +1 831 656 3686.
E-mail address: pcchu@nps.edu (P.C. Chu).
URL: http://www.oc.nps.navy.mil/~chu (P.C. Chu).

0924-7963/$ - see front matter © 2006 Elsevier B.V. All rights reserved.
doi:10.1016/j.jmarsys.2006.01.013

A fully spectral third-generation ocean wind–wave model, Wavewatch-III (henceforth denoted as WWATCH), is used to simulate the WBL parameters. The effects of WBL can be easily identified by the differences in (C_D, z_0) and DMS transfer velocity between with and without WBL. The outline of this paper is as follows: A description of SCS, Typhoon Wukong 2000, and WWATCH model is given in Sections 2, 3, and 4. Drag coefficient and roughness length are given in Section 5. The effects of WBL on the drag coefficient, roughness length and DMS transfer velocity are presented in Sections 6 and 7. In Section 8 the conclusions are presented.

2. South China Sea

The SCS is a semi-enclosed tropical sea located between the Asian land mass to the north and west, the Philippine Islands to the east, Borneo to the southeast, and Indonesia to the south, a total area of $3.5 \cdot 10^6$ km^2. Its southern border is 3° S between South Sumatra and Kalimantan (Karimata Straits), and its northern border is the Strait of Taiwan from the northern tip of Taiwan to the Southeast coast of China. All of the straits are shallow except Luzon Strait whose maximum depth is 1800 m. The elliptical shaped central deep basin is 1900 km along its major axis (northeast–southwest) and approximately 1100 km along its minor axis, and extends to over 4000 m deep.

The SCS can be viewed as a distinctive ecosystem due to its boundaries of archipelagoes and peninsulas, dotted by small islands and coral reefs; the striking variation in its sea floor characteristics, averaging 100 m deep on the continental Sunda shelf and over 5000 m in the Philippine basin; and its unusual monsoon weather patterns of reversing summer and winter rains and winds. The northeast monsoon between December and February and the southwest monsoon between June and August change the surface water circulation pattern. Geology and climate combine to produce a remarkable amount of biological diversity and immense genetic resources in the SCS. Extensive coral reefs support several thousand different species of organisms and play an important part in buffering wave impact on beaches, thus reducing erosion. The highly variable wind systems and complicated topography make SCS a perfect location for the investigation.

3. Typhoon Wukong 2000

Typhoon Wukong 2000 formed as a tropical depression west of Luzon Island at 06UTC on 4 September. It remained almost stationary until 12UTC on 5 September and then made an anticlockwise turn to the west (Fig. 1). During the turn the depression was developed into a tropical storm at 00UTC on 6 September. It further intensified to attain modest typhoon intensity at 18UTC on 7 September and reached its peak with estimated maximum sustained winds of 38 m s^{-1} at 06UTC on 8 September (Fig. 2). Weakening gradually, Wukong skirted around the southern coasts of Hainan Island on 9 September and made landfall on the northern part of Vietnam at around 04UTC on 10 September. After

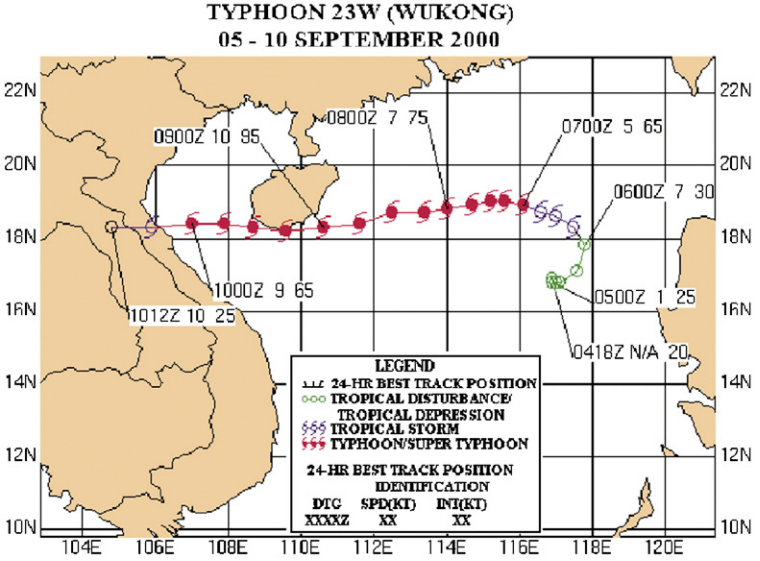

Fig. 1. Track of Typhoon Wukong 2000 during September 4–10, 2000.

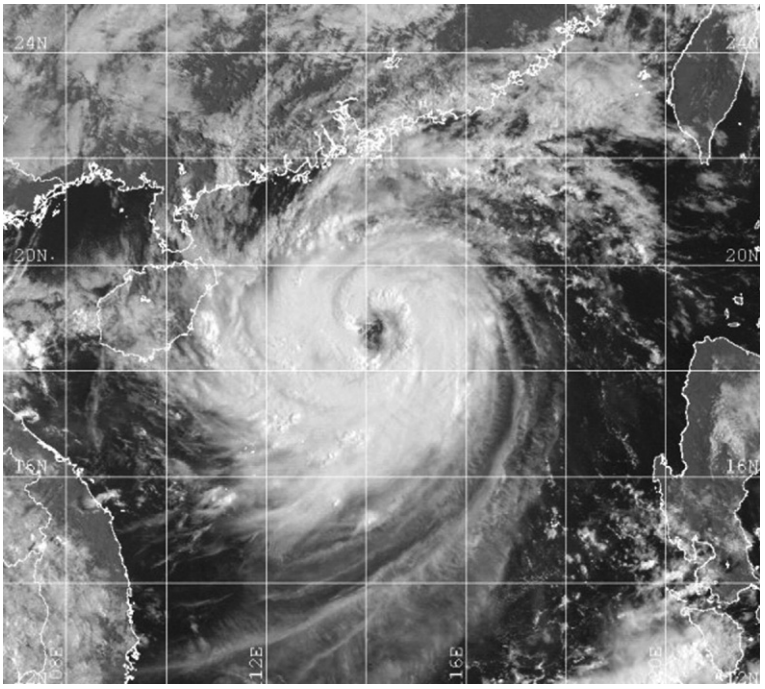

Fig. 2. GMS-5 visible image of Tyhoon Wukung at 0031Z on 8 September 2000 when the cyclone was located about 390 km east of Hainan Island and tracking westward. Evident outflow is seen in all quadrants as well as a clear but irregular eye.

the landfall it was weakened into a tropical depression in the northeastern part of Thailand at 12UTC on 10 September.

4. WWATCH model

4.1. Description

WWATCH was developed for regional sea wave prediction at the Ocean Modeling Branch of the Environmental Modeling Center of the National Centers for Environmental Prediction (NCEP). It was built on the base of Wavewatch-I and Wavewatch-II as developed at the Delft University of Technology and NASA Goddard Space Flight Center, respectively (Tolman, 1999). WWATCH implemented in the SCS has been evaluated using the significant wave height (SWH) data collected by satellites with altimetry, such as TOPEX/POSEIDON (T/P) (Chu et al., 2004). The SWHs from WWATCH are compared to that from T/P at the satellite crossover points in SCS. The model errors of SWH have Gaussian-type distribution with small mean value of 0.02 m (almost no bias). The model errors are comparable to the T/P altimeter accuracy (0.5 m) in the central SCS and smaller than the T/P altimeter accuracy in the northern and southern SCS, which indicates the capability of WWATCH for the SCS wave simulation.

Let (x, y) be the Cartesian coordinates with $(\mathbf{i}, \mathbf{j})$ the unit vectors. The wave spectrum F is generally a function of space ($\mathbf{x} = x\mathbf{i} + y\mathbf{j}$), time ($t$), and phase parameters (σ, k, θ, ω),

$$F = F(k, \theta, \sigma, \omega; \mathbf{x}, t), \tag{1}$$

where k is the wave number (unit: m^{-1}); θ is the direction (unit: degree); σ is the intrinsic frequency (unit: s^{-1}); and ω is the absolute frequency (unit: s^{-1}). The individual spectral components are assumed to satisfy the linear wave theory (locally) and to follow the dispersion relation,

$$\sigma^2 = gk \tanh kd, \quad \omega = \sigma + kU, \tag{2}$$

where d is the mean water depth; U is the (depth- and time-averaged) current velocity. When U is given, only two-phase parameters among $(\sigma, k, \theta, \omega)$ are independent. Many wave models use the frequency-direction (σ, θ) as the independent phase variables. However, WWATCH uses the wavenumber-direction (k, θ) as the independent phase variables.

Without currents, the energy of a wave package is conserved. With currents the energy of a spectral component is no longer conserved (Longuet-Higgins and Stewart, 1961), but the wave action spectrum,

$$N(k, \theta; \mathbf{x}, t) \equiv F(k, \theta; \mathbf{x}, t)/\sigma,$$

is conserved (Whitham, 1965; Bretherthon and Garrett, 1968). In WWATCH, the basic equation is for the wave action spectrum.

4.2. Model setting

WWATCH has two types (mandatory and optional) of model switches for users to choose. Table 1 lists the model setting and optional switches for this study. For example, spatial and spectral grids are user-defined; the quickest propagation scheme is selected with the dispersion correction (Booij and Holthuijsen, 1987); nonlinear interactions are included; and the source term parameterization includes wind input, nonlinear wave–wave interaction, dissipation, and wave-bottom interaction (Tolman and Chalikov, 1996).

4.3. Discretization

The model is implemented for SCS (0° to 25° N, 105°–122° E) with realistic bathymetry data from the Naval Oceanographic Office (i.e., DBDB5) and a regular longitude–latitude grid ($\Delta x = \Delta y = 25$ km). The wave direction (θ) is also regularly gridded with $\Delta\theta = 15°$. The wavenumber grid spacing is determined by the frequency intervals (total 25)

$$\sigma_{m+1} = X_\sigma \sigma_m, \qquad m = 0, 1, \ldots, 24, \tag{3}$$

with

$$X_\sigma = 1.1, \quad \sigma_0 = 0.0418. \tag{4}$$

Two time steps (300 s and 100 s) are used in WWATCH to reach computational efficiency: (a) global time step (300 s) for the propagation of the entire solution, (b) spatial time step (300 s) for the spatial propagation, (c) spectral time step (300 s) for intra-spectral propagation, and (d) source time step (100 s) for the source term integration.

Table 1
Model setting for this study

Switch parameters	Characteristics
DUM	Dummy to be used if WWATCH is to be installed on previously untried hardware
LRB8	8 byte words
SHRD	Shared memory model, no message passing
SEED	Seeding of high-frequency energy
GRD1	Settings directly hardwired to user-defined spatial grids (spherical coordinate with 0.25° grids)
SP1	User-defined spectral grids.
PR2	Ultimate quickest propagation scheme with Booij and Holthuijsen (1987) dispersion correction
ST2	Tolman and Chalikov (1996) source term package
STAB2	Enable stability correction for Tolman and Chalikov (1996) source term package
NL1	Nonlinear interaction (DIA)
BT1	JONSWAP bottom friction formulation
WIND2	Approximately quadratic interpolation
CUR2	Approximately quadratic interpolation
o1	Output of boundary points in grid preprocessor
o2	Output of the grid point status map in grid preprocessor
o2a	Generation of land–sea mask file mask.ww3 in grid preprocessor
o3	Additional output in loop over fields in field preprocessor
o4	Print plot of normalized 1-D energy spectrum in initial conditions program
o5	2-D energy spectrum
o6	Spatial distribution of wave heights (not adapted for distributed memory)
o7	Echo input data for homogeneous fields in generic shell

4.4. Model integration

WWATCH is integrated from the JONSWAP-1973 wave spectra (Hasselmann et al., 1980) with four-time daily reanalyzed NCEP winds ($1° \times 1°$) from January 1, 2000 to 31 December 2000. The output of WWATCH consists of the traditional frequency-direction spectrum $F(\sigma,\theta, \mathbf{x}, t)$, which is calculated from wavenumber-direction spectrum $F(k, \theta, \mathbf{x}, t)$ using the Jacobean transformation. The peak frequency (ω_p) and in turn the peak phase speed (c_p) can be determined for ($\mathbf{x}$, t) from the spectrum $F(\sigma,\theta, \mathbf{x}, t)$.

4.5. Model verification

SWH is chosen for model verification (Chu et al., 2004). The model-data comparison is conducted at all 20 crossover points in SCS. Each one contains approximately 72 pairs of modeled (H_m) and observed (H_o) SWH data in 2000. The total number of pairs is 1330. The model error is represented by the difference between the modeled and observed SWH at the crossover points, $\Delta H = H_m - H_o$.

Over the whole SCS, WWATCH has very low bias (−0.01 to 0.04 m) in predicting SWH with a maximum (positive bias) value of 0.04 m in March and a minimum (negative bias) value of −0.01 m in April. The root-mean-square error has a minimum value of 0.39 m in March and a maximum value of 0.48 m in December. The model errors are comparable to the T/P altimeter accuracy (0.5 m) in the central SCS and smaller than the T/P altimeter accuracy in the northern and southern SCS, which indicates the capability of WWATCH for SCS wave simulation. Interested readers are referred to Chu et al. (2004).

5. Drag coefficient and roughness length

The mean wind profile is represented by

$$u(z) = \frac{u*}{\kappa} \ln\left(\frac{z}{z_0}\right), \tag{5}$$

where $\kappa = 0.4$ is the von Karman constant and $u*$ is the air friction velocity, which is defined by

$$C_D = u_*^2 / u_r^2. \tag{6}$$

where C_D is the drag coefficient of the ocean surface. C_D was originally considered as a constant (e.g., Kraus, 1972). However, as the quantity and quality of measurements have improved, it became evident that C_D tends to increase with increasing wind speed (e.g., Garratt, 1977).

Using Eqs. (5) and (6), the roughness length z_0 becomes

$$z_0 = z_r \exp\left(-\frac{\kappa}{\sqrt{C_D}}\right). \tag{7}$$

The roughness length is also expressed in the dimensionless form

$$z_{0*} = z_0 g / u_*^2, \tag{8}$$

where g is the gravitational acceleration, and the dimensionless roughness z_{0*}, is generally referred to as the Charnock parameter. Without WBL, the Charnock parameter is considered as a constant (e.g., Charnock, 1955),

$$z_{0*} = 0.0144. \tag{9}$$

For the given wind speed at the reference height z_r ($z_r = 10$ m in this study), the drag coefficient C_D, roughness length z_0, and the friction velocity u_* can be obtained through the iteration using Eqs. (6)–(9). The iteration stops when the relative change of the friction velocity is smaller than a prescribed criterion (10^{-3}). Such iterations are performed during the model initialization, but are not necessary during the actual model run as $u*$ changes slowly (Tolman and Chalikov, 1996; Tolman, 1999). The effect of the atmospheric instability on the friction velocity is parameterized using an effective wind speed u_e(Tolman and Booij, 1998), which depends on the surface air and sea temperature difference.

6. Effect of WBL on drag coefficient and roughness length

Field data indicate convincingly that C_D is sea state dependent (Hwang, 2005). The WBL is the lower part of the atmospheric boundary layer above the sea, whose structure is influenced directly by surface waves. Within the WBL, some portion of momentum transfer results from wave-produced fluctuations of pressure, velocity, and stresses. The drag coefficient C_D at the reference height z_r is calculated by (Charlikov, 1995)

$$C_D = \kappa^2 [R - \ln C_D]^2, \tag{10}$$

$$R = \ln\left(\frac{z_r g}{\gamma \sqrt{\mu_p \mu_r}}\right), \tag{11}$$

where $\gamma = 2$ is a constant; μ_p is the conventional nondimensional energy level at peak frequency (ω_p). Estimation of the drag coefficient thus requires an estimate of the energy level μ_p at peak frequency, which is parameterized by (Janssen, 1989),

$$\mu_p = 0.57 \left(\frac{u*}{c_p}\right)^{3/2}, \tag{12}$$

Obviously, μ_p also depends on the drag coefficient C_D. Thus, the iteration should be conducted to get (C_D, z_0, u_*) using Eqs. (10)–(12). During the iteration, the peak phase speed c_p in Eq. (12) is obtained from the WWATCH simulated wave spectrum (F).

Fig. 3 shows the scatter diagram of the Charnock parameter z_{0*} versus the nondimensional peek angular frequency ω_{p*} ($=\omega_p u_* / g$) with WBL during the passage of Typhoon Wukong (4–10 September 2000). The points are deviated a lot from the horizontal line,

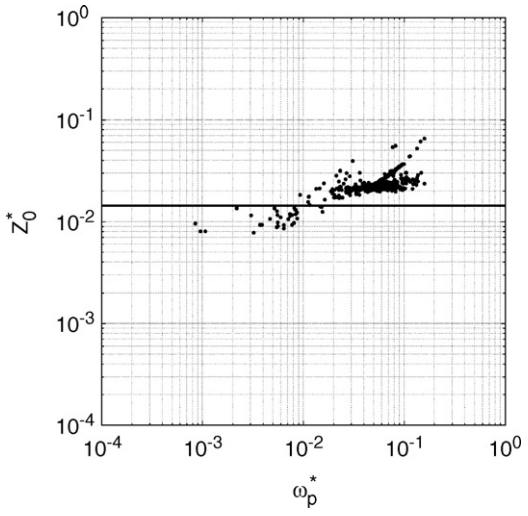

Fig. 3. Comparison of the Charnock parameter z_{0*} without WBL (solid line) and with WBL (dots) for the northern SCS (15°–25° N) during 5–10 September, 2000. Here, $\omega_p^* \equiv \omega_p u_* / g$ with ω_p the angular peek frequency.

z_{0*}=0.0144 (without WBL), which indicates the large effect of WBL on the roughness length. The horizontally averaged drag coefficient (Fig. 4) over the northern SCS (15°–25° N) is evidently larger with WBL ($C_D^{(w)}$, solid curve) than without WBL ($C_D^{(n)}$, dashed curve).

The relative increase of the drag coefficient due to WBL is calculated by

$$\delta = \frac{\sum_i \sum_j \left[C_D^{(w)}(i,j) - C_D^{(n)}(i,j) \right]}{\sum_i \sum_j C_D^{(n)}(i,j)}, \quad (13)$$

where the summation is over the total number of grid points in the northern SCS (15°–25° N). The parameter δ generally increases with the intensity of Typhoon Wukong (Fig. 5). As the low pressure of the typhoon reaches its minimum value of 955 hPa on September 8, δ has its maximum value of 16.5%. A recent study shows reduced drag coefficient for high wind speeds (>40 m s^{-1}) in tropical cyclones (Powell et al., 2003). However, Wukong 2000 is a modest typhoon with maximum sustained winds of 38 m s^{-1}. The simulated enhancing WBL effect (on drag coefficient) with wind speed during the passage of Wukong 2000 does not conflict with Powell et al.'s (2003) results.

7. Effect of WBL on DMS transfer velocity

The sea-to-air DMS flux exhibits more complexity than the bulk aerodynamic relations described in the previous sections. Turbulent transfer in the atmosphere above the surface plays a key role, but chemical properties of the surface and/or reactions with sea spray are also important. For chemical compounds which react

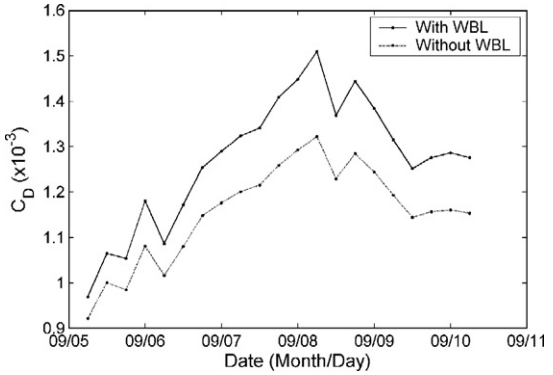

Fig. 4. Comparison of temporally varying horizontal averaged C_D without WBL (dotted curve) and with WBL (solid curve) for the northern SCS (15°–25° N) during 5–10 September, 2000.

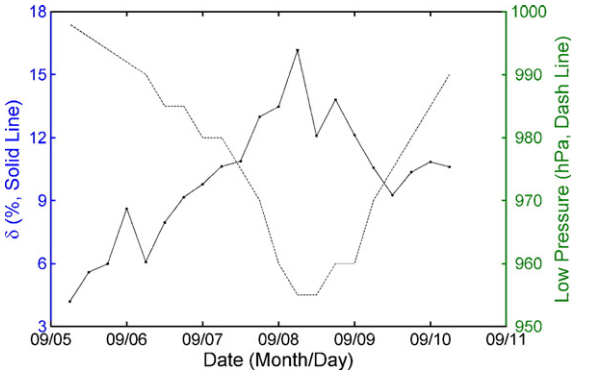

Fig. 5. Temporally varying relative increase of C_D between with and without WBL (solid curve) for the northern SCS (15°–25° N) and typhoon intensity (dashed curve) represented by minimum pressure. Note that the increase can reach 16.5% on 8 September 2000 when the typhoon Wukong is strongest.

with sea spray aerosols (e.g., ammonia and nitric acid), the constant flux layer assumption may not be valid; and additional equations must be considered. For chemical compounds with reaction time scales longer than the surface layer turbulence time scales, the constant flux layer assumption may be invoked. This applies to gases such as DMS. It is noted that the photo reactions (same time scale as the turbulence) are not considered here. The sea-to-air DMS flux (H) is characterized by transfer velocities k_a and k_w (McGillis et al., 2000),

$$H = \frac{k_w}{1 + \alpha k_w / k_a} (C_w - \alpha C_a), \quad (14)$$

where C_a and C_w are the bulk concentrations in the air and water; α is the Ostwald solubility coefficient for DMS,

$$\alpha = \exp\left[\frac{3525}{T} - 9.464 \right], \quad (15)$$

where T is temperature (in K). Waterside transfer velocity (k_w) is parameterized by (Jahne et al., 1987; McGillis et al., 2000)

$$k_w = \sqrt{\rho_a / \rho_w}\, \beta^{-1} Sc^{-n} u_*, \quad (16)$$

where (ρ_a=1.29 kg m^{-3}, ρ_w=1025 kg m^{-3}) are the characteristic air and water densities; β is the dimensionless Stanton number showing the resistance to momentum transfer across the water-side viscous boundary layer; and

$$Sc = \nu / D, \quad (17)$$

is the Schmidt number. Here, ν is the kinematic viscosity for momentum, and D is the diffusion coefficient for gas

transfer. The diffusion coefficient of DMS is calculated by (Saltzman et al., 1993)

$$D = 1.1 \times 10^{-2} \exp\left[-\frac{1896}{T}\right] (\text{unit} : \text{cm}^2\text{s}^{-1}). \quad (18)$$

The Schmidt number for DMS at 300 K is taken as (Saltzman et al., 1993),

$$Sc = 720. \quad (19)$$

The kinetic viscosity of DMS can be calculated from D and Sc using Eqs. (17)–(19).

Airside transfer velocity (k_a) is calculated by

$$k_a = k_{H_2O}(M/M_{H_2O})^{-1/2}, \quad (20)$$

where M (=62.129) and M_{H_2O} (=18.015) are the molecular weights for DMS and H_2O; k_{H_2O} is the water vapor transfer velocity which is calculated by

$$k_{H_2O} = 659 u_r. \quad (21)$$

In fully rough regime of the sea state such as the case discussed in this paper (wave generation during the typhoon passage), the exponent in Eq. (16) is given by n=0.58; and the Stanton number is represented by (Jahne et al., 1987)

$$\beta = 0.55 Re_r^{1/4}, \quad (22)$$

where

$$Re_r \equiv u_* z_0 / \nu, \quad (23)$$

is the roughness Reynolds number.

The horizontally averaged DMS transfer velocity (k_w) over the northern SCS (Fig. 6) is evidently smaller

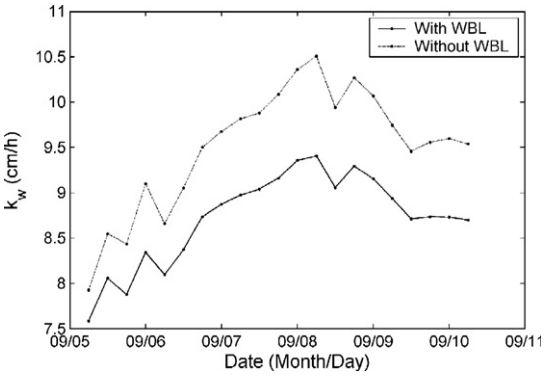

Fig. 6. Comparison of temporally varying horizontal averaged waterside transfer velocity k_w without WBL (dotted curve) and with WBL (solid curve) for the northern SCS (15°–25° N) during 5–10 September, 2000.

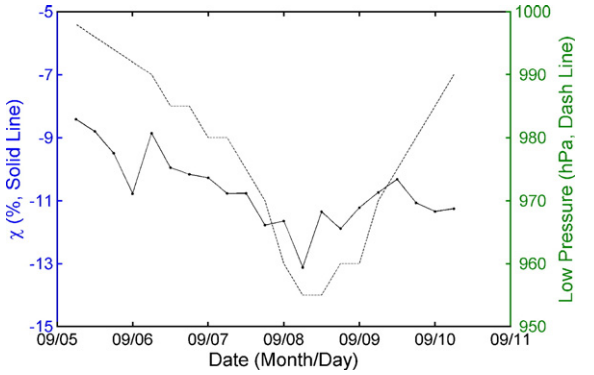

Fig. 7. Temporally varying relative decrease of waterside transfer velocity k_w between with and without WBL (solid curve) for the northern SCS (15°–25° N) and typhoon intensity (dashed curve) represented by minimum pressure. Note that the relative decrease of waterside transfer velocity follows the intensity of Typhoon Wukong. It reaches −13.1% on 8 September 2000 (strongest strength of typhoon Wukong).

with WBL ($k_w^{(w)}$, solid curve) than without WBL ($k_w^{(n)}$, dashed curve). The relative decrease of the transfer velocity due to WBL is calculated by

$$\chi = \frac{\sum_i \sum_j \left[k_w^{(w)}(i,j) - k_w^{(n)}(i,j)\right]}{\sum_i \sum_j k_w^{(n)}(i,j)}. \quad (24)$$

The parameter χ generally decreases with the intensity of Typhoon Wukong (Fig. 7). As the low pressure of the typhoon reaches its minimum value of 955 hPa on September 8, the value of χ has its minimum of −13.1%.

8. Conclusions

(1) Effects of wave boundary layer on the drag coefficient and the sea-to-air transfer velocity of dimethylsulfide (DMS) are investigated using the third generation wave model (Wavewatch-III) implemented in the South China Sea during passage of Typhoon Wukong 2000. The model was verified using the significant wave height measured by TOPEX/POSEIDON altimeter for 2000 (Chu et al., 2004). Without the wave boundary layer, the drag coefficient and the DMS transfer velocity are independent on the wave spectra. With the wave boundary layer, the drag coefficient and the sea-to-air DMS transfer velocity are dependent on the wave spectra.

(2) The drag coefficient is larger with the wave boundary layer than without the wave boundary layer. Such a drag coefficient difference increases with the intensity of the typhoon (in turns with the wave energy). It is only 4% on September 5 when the minimum pressure of Typhoon Wukong is 998 hPa, and monotonically increases to 16.5% on September 8 when the minimum pressure of Typhoon Wukong is 955 hPa.

(3) The DMS transfer velocity is smaller with the wave boundary layer than without the wave boundary layer. Such transfer velocity difference enhances with the typhoon intensity (in turns with the wave energy). It is only 8.3% on September 5 when the minimum pressure of Typhoon Wukong is 998 hPa, and increases to 13.1% on September 8 when the minimum pressure of Typhoon Wukong is 955 hPa.

(4) For a modest typhoon such as Wukong 2000 (maximum sustained winds of 38 m s^{-1}), the wave boundary layer shows the evident impacts (i.e., enhancing the momentum and reducing the sea-to-air DMS flux). These features are identified using Chalikov's (1995) parameterization of the wave boundary layer and McGillis et al.'s (2000) parameterization of waterside transfer velocity. The same results (not shown here) are also obtained using other parameterizations (e.g., Asman et al., 1994). Therefore, further investigation is needed on the effects of the wave boundary layer on atmospheric DMS contents and global climate system.

Acknowledgements

The authors wish to thank Dr. Tolman at the National Weather Service for providing the Wavewatch-III model, *the NOAA-CIRES Climate Diagnostics Center for providing NCEP Reanalysis data,* and NASA/JPL for providing TOPEX/POSEIDON data. This work was jointly funded by the Naval Oceanographic Office, and the Naval Postgraduate School.

References

Asman, W.A.H., Harrison, R.M., Otley, C.J., 1994. Estimation of the net air–sea flux of ammonia over the southern bight of the North Sea. Atmos. Environ. 28 (22), 3647–3654.

Bates, T.S., Lamb, B.K., Guenther, A.B., Dignon, J., Stoiber, R.E., 1992. Sulfur emissions to the atmosphere from natural sources. J. Atmos. Chem. 14, 315–337.

Booij, N., Holthuijsen, L.H., 1987. Propagation of ocean waves in discrete spectral wave models. J. Comput. Phys. 68, 307–326.

Bretherthon, F.P., Garrett, C.J.R., 1968. Wave trains in inhomogeneous moving media. Proc. R. Soc. Lond., A 302, 529–554.

Charlikov, D., 1995. The parameterization of the wave boundary layer. J. Phys. Oceanogr. 25, 1333–1349.

Charnock, H., 1955. Wind stress on water surface. Q. J. R. Meteorol. Soc. 81, 639–640.

Chu, P.C., Qi, Y.Q., Chen, Y.C., Shi, P., Mao, Q.W., 2004. South China Sea wave charcteristics. Part-1: validation of wavewatch-III using TOPEX/Poseidon data. J. Atmos. Ocean. Technol. 21 (11), 1718–1733.

Garratt, J.R., 1977. Review of drag coefficients over oceans and continents. Mon. Wea. Rev. 105, 915–929.

Gondwe, M., Krol, M., Gieskes, W., Klaassen, W., de Baar, H., 2003. The contribution of ocean-leaving DMS to the global atmospheric burdens of DMS, MSA, SO_2 and NSS SO_4. Glob. Biogeochem. Cycles 17, 1056, doi:10.1029/2002GB001937.

Hasselmann, D.E., Dunckel, M., Ewing, J.A., 1980. Directional wave spectra observed during JONSWAP 1973. J. Phys. Oceanogr. 10, 1264–1280.

Hwang, P.A., 2005. Temporal and spatial variation of the drag coefficient of developing sea under steady wind-forcing. J. Geophys. Res.-Oceans 110, C07024, doi:10.1029/2005JC002912.

Kraus, E.B., 1972. Atmosphere–Ocean Interaction. Oxford University Press, p. 275.

Jahne, B., Munnich, K.O., Bosinger, R., Dutzi, A., Huber, W., Libner, P., 1987. On the parameters influencing air–water gas exchange. J. Geophys. Res.-Oceans 92, 1937–1949.

Janssen, P.A.E.M., 1989. Wave-induced stress and the drag of air flow over sea waves. J. Phys. Oceangr. 19, 745–754.

Longuet-Higgins, M.S., Stewart, R.W., 1961. The changes in amplitude of short gravity waves on steady non-uniform currents. J. Fluid Mech. 10, 529–549.

McGillis, W.R., Dacey, J.W.H., Frew, N.M., Bock, E.J., Nelson, R.K., 2000. Water–air flux of dimethylsulfide. J. Geophys. Res.-Oceans 105, 1187–1193.

Powell, M.D., Vickery, P.J., Reinhold, T.A., 2003. Reduced drag coefficient for high wind speeds in tropical cyclones. Nature 422, 279–283.

Saltzman, E.S., King, D.B., Holmen, K., Leck, C.J., 1993. Experimental determination of the diffusion coefficient of dimethylsulfide in water. J. Geophys. Res.-Oceans 98, 16481–16486.

Tolman, H.L, 1999. User manual and system documentation of WAVEWATCH-III version 1.18. NOAA/NCEP Technical Note, vol. 166, p. 110.

Tolman, H.L., Booij, N., 1998. Modeling wind waves using wavenumber-direction spectra and a variable wavenumber grid. Global Atmos. Ocean Syst. 295–309.

Tolman, H.L., Chalikov, D.V., 1996. Source terms in a third-generation wind wave model. J. Phys. Oceanogr. 26, 2497–2518.

Whitham, G.B., 1965. A general approach to linear and non-linear dispersive waves using a Lagrangian. J. Fluid Mech. 22, 273–283.